JOURNAL OF GEOPHYSICAL RESEARCH, VOL. 93, NO. C12, PAGES 15,523–15,533, DECEMBER 15, 1988

Modification of Ocean Eddies by Air-Sea Interaction

RICHARD G. WILLIAMS

Space and Atmospheric Physics Group, Department of Physics, Imperial College, London

A mixed-layer model is developed for seasonal time scales and used to investigate the modification of ocean eddies by air-sea interaction. An eddy is modified by the air-sea interaction for the local envionment and the feedback from its surface temperature signal, which alters the surface heat and water fluxes. This buoyancy forcing tends to decrease the eddy temperature anomaly, and seasonal changes in mixed-layer depth lead to the surface signal being removed in summer and reappearing in winter. The dynamical adjustment of the eddy is assessed by coupling the mixed-layer model to a quasi-geostrophic model: the buoyancy forcing alters the eddy velocity profile and, over several seasons, may lead to the formation of a subsurface velocity maximum. After the spring decrease in mixed-layer depth, the eddy potential vorticity anomaly is reduced, and lateral mixing may subsequently play a role in further eroding the eddy. These modelling predictions are supported by the observations of a cold-core eddy in the seasonal boundary layer of the northeast Atlantic.

1. INTRODUCTION

Ocean synoptic-scale eddies are principally formed by internal instability of the vigorous western boundary currents [*Richardson*, 1983]. The weaker mid-ocean eddy field may be generated by a variety of mechanisms: movement of eddies from the boundary currents, baroclinic instability in the open ocean [*Gill et al.*, 1974], mean flow interaction with bottom topography and perhaps transient wind stress forcing [*Müller and Frankignoul*, 1981]. An eddy acquires a water mass structure typical of its formation region. The eddy may subsequently move into a different region due to a combination of mean flow advection and self-propagation [*Davey and Killworth*, 1984]. In this new environment, the eddy appears as an anomalous water mass with a sea surface temperature signal.

Ocean eddies are modified by air-sea interaction in the seasonal boundary layer through solar heating and the exchange of heat, moisture, and momentum. This modification of an eddy depends on the air-sea interaction for the local environment and on the feedback from its surface temperature signal, which alters the surface heat and water fluxes. This process may become important in determining the eddy structure over a seasonal time scale, if the eddy escapes being absorbed and destroyed in the western boundary currents.

The influence of air-sea interaction on ocean eddies is investigated by examining a cold-core eddy detected in the seasonal boundary layer of the northeast Atlantic (section 2). The possible changes in an eddy during its lifetime are investigated further by applying a mixed-layer model (section 3) and integrating it for both the eddy and the local environment (section 4); this extends the work of *Schmitt and Olson* [1985] on wintertime convection in a warm-core Gulf Stream ring and that of *Dewar* [1986] on seasonal changes of warm- and cold-core Gulf Stream rings. The dynamical changes in an eddy are then assessed by solving the quasi-geostrophic potential vorticity equation using realistic diabatic forcing deduced from the mixed-layer integrations (section 5).

Paper number 88JC03027.
0148–0227/88/88JC–03027$05.00

2. A COLD-CORE EDDY OBSERVED IN THE SEASONAL BOUNDARY LAYER

2.1. Observations of the Cold-Core Eddy

A cold-core eddy was detected during the summer of 1983 by the FS *Poseidon* 101b cruise in the northeast Atlantic [*Leach et al.*, 1987]. This single section of hydrographic and velocity data extends for 650 km in the seasonal boundary layer from 43.6°N, 28.2°W to 48.8°N, 32.1°W and covered the period 0800 GMT June 26 to 2000 GMT June 27,1983 (Figure 1). The hydrographic data were collected by a towed fish, multisonde system which oscillated from the surface to a depth of 60 m [*Leach et al.*, 1985]. The velocity data were taken from an electromagnetic log instrument and a Doppler-sonar current profiler at depths of 5 m and 50 m, respectively.

The cold-core eddy is revealed by the low temperature and salinity signals on σ_t surfaces (Figure 2), which extend for approximately 120 km along the section. The center of the eddy was observed at 46.3°N, 30.2°W and a time of 0200 GMT June 27, 1983. The eddy core extends for 40 km and is cooler and fresher by -1.2 ± 0.1 °C and -0.33 ± 0.04 than the local environment along the $\sigma_t = 26.7$ surface. On either side of the eddy core, the temperature and salinity gradients are an order of magnitude larger than the mean gradients along the section. In these frontal regions, there is some finer structure in which the gradients reverse with a length scale of the order of 10 km: this may be due to lateral mixing between the eddy and the surrounding environment.

The cold-core eddy is associated with a cyclonic circulation in both sets of velocity data (Figure 3). The eddy velocity maxima of 58 cm/s occur within the temperature frontal regions, and the maximum horizontal shear is inside the anomalous core. If the eddy is taken to be cylindrically symmetric, then the Rossby number is 0.27 and 0.33 at depths of 5 m and 50 m respectively. The geostrophic shear (perpendicular to the section) deduced from the depth of σ_t surfaces shows that the cyclonic signal is weaker by 3.5 cm/s at the surface than at a depth of 60 m. The observed eddy

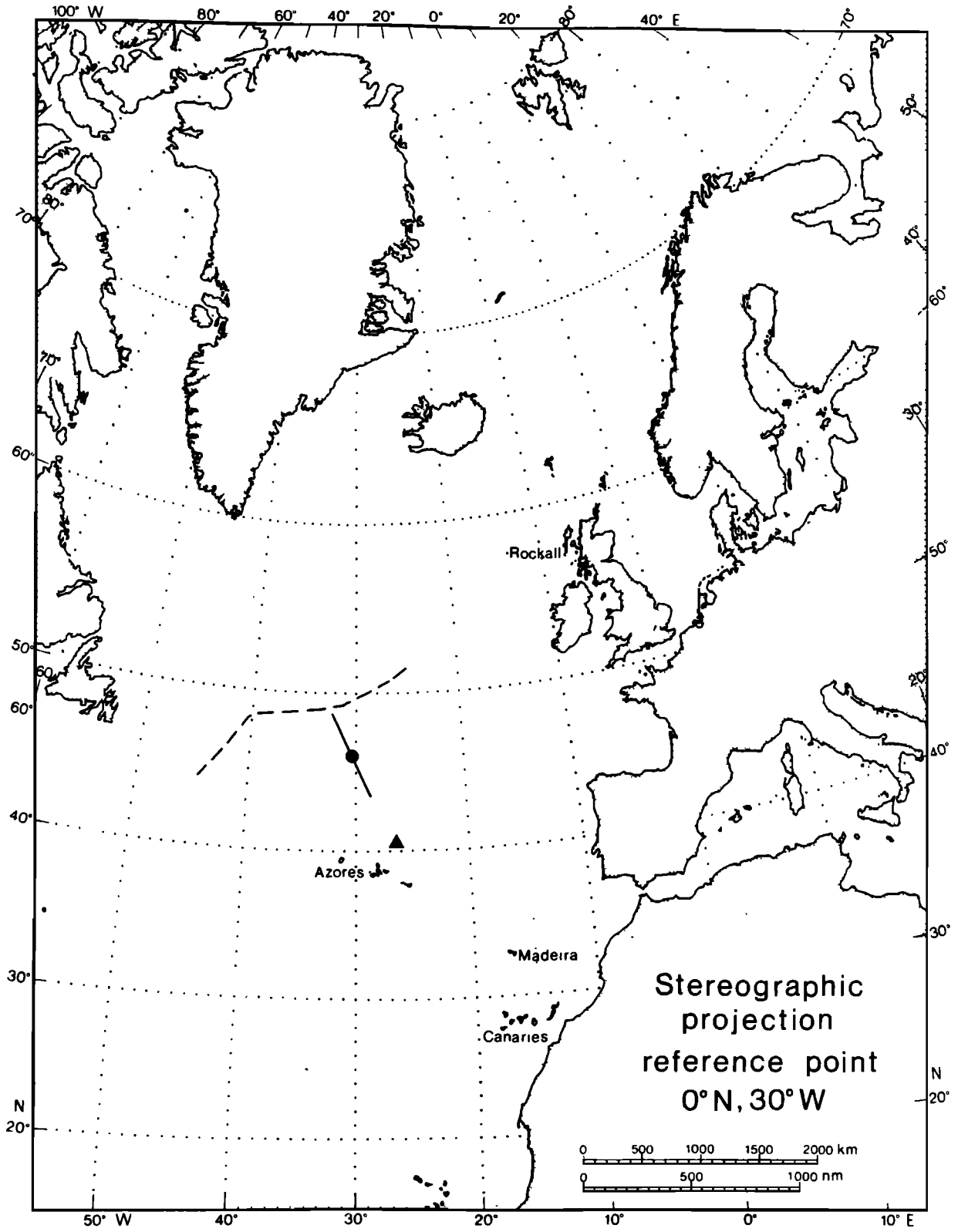

Fig. 1. The northeast Atlantic in a stereographic projection [*Woods*, 1984]. A cold-core eddy is observed at 46.3°N, 30.2°W (circle) along a section of the FS *Poseidon* 101b cruise (solid line): its salinity signal suggests that it originates from the north or west (dashed line). A mixed-layer model is run at a site 40.5°N, 26.5°W (triangle).

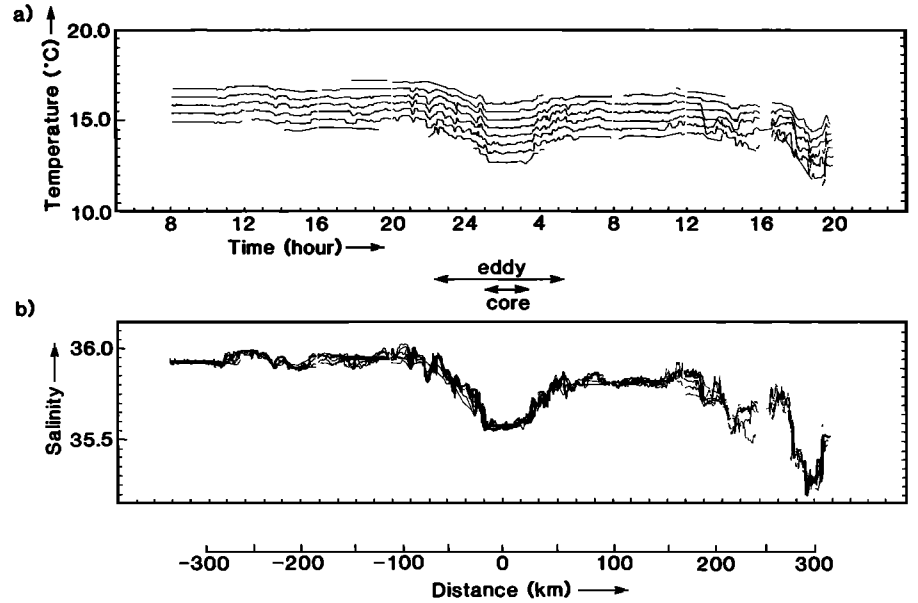

Fig. 2. Observed (a) temperature and (b) salinity values on σ_t surfaces, every 0.1 from 26.2 to 26.9, along the *Poseidon* section. An eddy is revealed by the cool, fresh water mass anomaly; the distance from its center is shown along the horizontal axis.

circulation (with velocities reaching 58 cm/s) is therefore due to either a deeper baroclinic signal or a barotropic signal.

The cold-core eddy is also associated with an increase in potential vorticity,

$$Q = -\frac{(\zeta + f)}{\rho}\frac{\partial \rho}{\partial z} \quad (1)$$

Here, ζ is the relative vorticity, ρ is the density, f is the Coriolis parameter, and z is the vertical coordinate. On the deeper σ_t surfaces, the eddy potential vorticity is twice as large as the mean values along the section (Figure 4). The potential vorticity maximum is due to both the smaller vertical spacing between isopycnals and the cyclonic relative vorticity, which accounts for 30% of the increase.

The eddy potential vorticity and density are nearly conserved below the mixed layer where diabatic changes are relatively small. Therefore, lateral mixing around the eddy is inhibited by the presence of the potential vorticity anomaly along density surfaces. Air-sea interaction may eventually reduce the potential vorticity anomaly in the seasonal boundary layer. Lateral mixing of typically 100 m^2/s [*Colin de Verdiere et al.*, 1986] should then become important and remove the remaining eddy salinity anomaly after an e-folding time scale of 130 days.

2.2. Formation and Movement of the Cold-Core Eddy

The cold-core eddy has a horizontal length scale of 34 km, as revealed from the temperature, salinity, and potential vorticity fields along the section (defined here as the distance for the anomaly to decrease by a factor of $1/e$). This horizontal length scale is near the preferred scale for baroclinic instability at the internal Rossby deformation radius $L_d = NH/f$; this is the order of 30 km for a depth scale of $H \sim 1$ km, a mean Brunt-Väisälä frequency of $N \sim 0.003$ s^{-1}, and $f \sim 10^{-4}$ s^{-1}. The cold-core eddy may have been formed by this instability process either in the open ocean or along a boundary current (where there are larger horizontal density gradients).

The cold-core eddy is unlikely to have been generated locally (at 46.3°N, 30.2°W), since it is associated with significant salinity and potential vorticity anomalies: its salinity anomaly of −0.33 over a depth of 60 m would require a surface water input of 0.6 m, whereas the local water flux into the ocean is only −0.2 m/yr [*Baumgartner and Reichel*, 1975]. Instead, the eddy probably developed in a cooler and fresher environment and then moved to the observed location in late June.

The salinity signal implies that the eddy originated from a source region ranging from between 46.3°N, 42.3°W and 49.7°N, 30.2°W (dashed line in Figure 1): hence the nearest possible formation site is 370 km away at 49.2°N, 32.6°W (using the climatological atlas of *Robinson et al.* [1979]). The potential vorticity of the eddy is also characteristic of a region to the north of latitude 49°N (using the Geochemical Ocean Sections Study cruise data along 42°W [*McDowell et al.*, 1982]). The eddy probably acquires the observed potential vorticity values (along $\sigma_t = 26.7$) in early May when the mixed layer becomes shallower than 60 m (see section 5.3). This implies that the eddy must have had a translational velocity of approximately 8 cm/s in order to move from the source region in early May to the observed location in late June (Figure 5).

2.3. Air-Sea Interaction of the Cold-Core Eddy

Air-sea interaction should decrease the surface signal of the cold-core eddy through additional surface heating. The eddy does not appear to have a clear surface temperature signal, as it is not evident in an infrared satellite picture taken 4 days after the hydrographic observations. In fact, the observed eddy temperature anomaly increases with depth from −0.6°C at 10 m to −2.0°C at 60 m (Figure 6*a*);

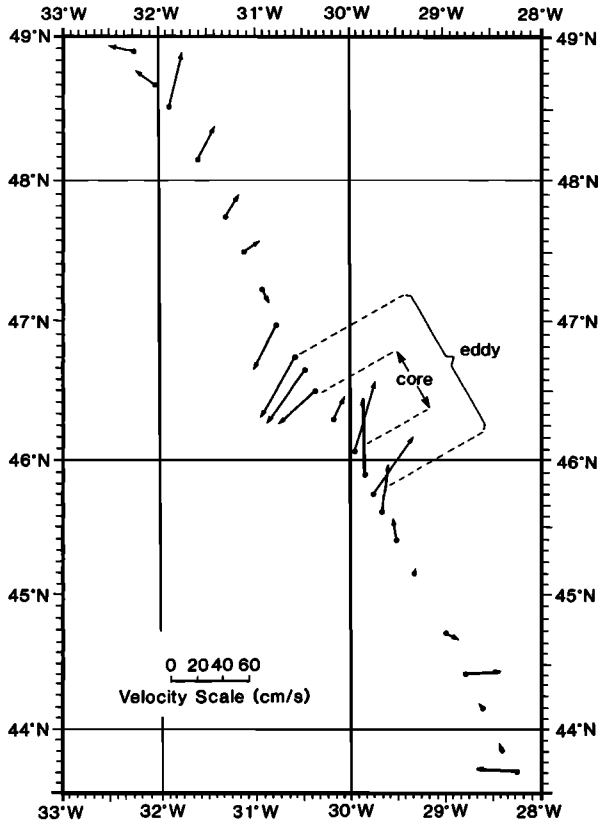

Fig. 3. Observed velocities along the *Poseidon* section at a depth of 50 m in a Mercator projection. The cold-core eddy detected in the water mass observations is associated with a cyclonic circulation.

these differences are between profiles in the eddy core and those interpolated from the background environment.

Additional surface heating of a cold-core eddy may produce a shallower mixed layer. The observed mixed-layer depth of 9 m in the eddy is indeed less than the mean value of 14 m along the section (defined here by a temperature decrease of 0.9°C from the surface). However, there are other

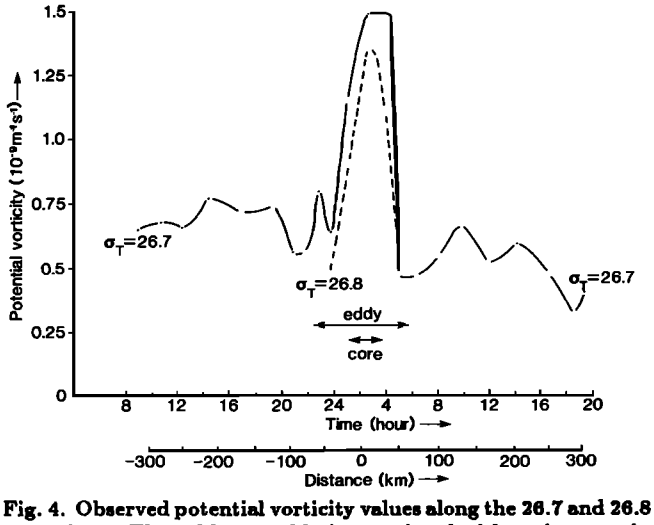

Fig. 4. Observed potential vorticity values along the 26.7 and 26.8 σ_t surfaces. The cold-core eddy is associated with an increase in potential vorticity; the distance from its center is shown along the horizontal axis.

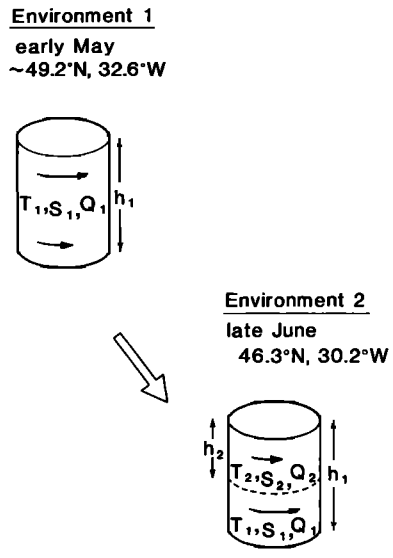

Fig. 5. Schematic movement of the cold-core eddy from a possible location in early May to the observed location in late June; T, S, Q, and h are the temperature, salinity, potential vorticity, and mixed-layer depth values for each site.

shallow mixed layer regions along the section which are not associated with changes in water mass.

Air-sea interaction should decrease the temperature anomaly of the cold-core eddy, but is unlikely to significantly alter the opposing salinity anomaly. The decrease in the temperature anomaly towards the surface leads to a reversal in the horizontal density gradient between the eddy and the local environment (Figure 6*b*); hence there should be a subsurface maximum in the geostrophic flow. The eddy cyclonic velocity field does indeed decrease towards the surface in both the direct velocity observations and the geostrophic flow deduced from the depth of σ_t surfaces.

In conclusion, air-sea interaction may have modified the structure of the cold-core eddy. The additional surface heating may have produced a shallower mixed layer, decreased the surface temperature signal and formed the subsurface velocity maximum. These hypotheses are examined further by developing a mixed-layer model and integrating it for an ocean eddy and the local environment.

3. Air-Sea Interaction for the Ocean Environment

3.1. Mixed-Layer Model Formulation

A one-dimensional, *Kraus and Turner* [1967] type mixed-layer model is used to examine seasonal changes in the upper ocean. The model does not include horizontal advection and vertical motion, and thus is only appropriate either for a Lagrangian frame or for locations where these processes are unimportant on an annual time scale. The model integrates the density and turbulent kinetic energy equations for seasonal time scales [*Niiler and Kraus*, 1977]:

$$\frac{\partial \bar{\rho}}{\partial t} + \frac{\partial}{\partial z}\overline{w'\rho'} = \frac{\alpha}{C_w}\frac{\partial I}{\partial z} \tag{2}$$

$$\frac{\partial E_a}{\partial t} = g\int_{-h}^{0} \overline{w'\rho'}\, dz \tag{3}$$

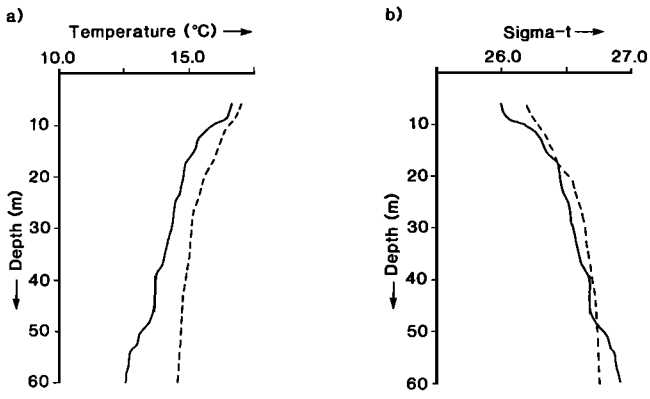

Fig. 6. Observed profiles of (a) temperature and (b) σ_t in the cold-core eddy (solid line) and the background environment (dashed line); these are interpolated from the surrounding values (at ±100 km) along the *Poseidon* section.

The density changes are controlled by (1) the divergence of the vertical density flux $\overline{w'\rho'}$, and (2) the solar heating I profile, (equation (2)). The vertical density flux depends on the surface heat and water fluxes, and the entrainment at the base of the mixed-layer. The mixed-layer depth h is calculated from the turbulent kinetic energy budget for seasonal time scales and depends on (1) the rate of production of available turbulent kinetic energy E_a, and (2) the rate of conversion to potential energy, (equation 3). Here, C_w is the heat capacity of water, g is gravity, and α is the density expansion coefficient for temperature. These coupled equations are solved numerically with the water column resolved into discrete depth layers. The density field is changed every time step by (1) solar heating, surface heat and water fluxes, (2) convective overturning, and (3) turbulent mixing.

3.2. Mixed-Layer Model Parameterizations

3.2.1. Solar heating, surface heat and water fluxes. The imposed solar radiation is calculated every hour from the solar zenith angle using monthly cloud cover and albedo [*List*, 1966; *Payne*, 1972; *Budyko*, 1974; *Bunker*, 1976]. The solar heating is applied throughout the water column using an empirical profile from a three-exponential fit with constant ocean turbidity (between Jerlov *IB* and *II*) [*Dickson*, 1972; *Horch et al.*, 1983].

The surface density flux depends on the surface heat and water fluxes:

$$\overline{w'\rho'}_{z=0} = -\frac{\alpha}{C_w}(Q_{ir} + Q_{le} + Q_{sens}) + \beta(P_w - F_w)S_o \quad (4)$$

Here, the surface fluxes are evaporation F_w, precipitation P_w, infrared radiation Q_{ir}, latent heat Q_{le}, and sensible heat Q_{sens}; S_o is the mean salinity, and β is its density contraction coefficient. The imposed surface heat and water fluxes are interpolated from monthly and seasonal data of *Bunker* [1976], and *Dorman and Bourke* [1981].

The density flux at the base of the mixed layer depends on the entrainment of deeper, denser fluid:

$$\begin{aligned} &\text{for shallowing} \quad \overline{w'\rho'}_{z=-h} = 0 \\ &\text{for deepening} \quad \overline{w'\rho'}_{z=-h} = \Delta\rho\frac{dh}{dt} \end{aligned} \quad (5)$$

where $\Delta\rho$ is the density jump at the base of the mixed layer.

3.2.2. Turbulent kinetic energy balance. The available turbulent mixing energy E_a comes from wind mixing E_w and penetrative convection E_c, and there is some loss through dissipation E_d:

$$E_a = E_w + E_c - E_d \quad (6)$$

The wind mixing energy depends on the imposed wind speed u_a, which is estimated from the monthly Bunker data set:

$$\frac{\partial E_w}{\partial t} = \rho_a c_d m_a u_a^3 \quad (7)$$

Here, c_d is the drag coefficient [*Large and Pond*, 1981], $m_a = 1.5 \times 10^{-3}$ is the efficiency of wind mixing [*Kato and Phillips*, 1969], and ρ_a is the air density.

Penetrative convection is assumed to occur whenever the surface cooling and evaporation produces a statically unstable density profile. The available turbulent kinetic energy is increased after overturning by a proportion $n = 0.15$ of the released potential energy ΔPE [*Gill and Turner*, 1976]:

$$E_c = n\Delta PE \quad (8)$$

The wind mixing energy is chosen to be dissipated exponentially with depth [*Wells*, 1979]:

$$E_d = E_w(1 - e^{-h/h_d}) \quad (9)$$

where h is the previous mixed-layer depth and h_d is the dissipation scale (chosen here to be 140 m).

The mixed-layer depth is calculated from the turbulent kinetic energy equation (3) by comparing the available energy E_a with the increase in potential energy required for entrainment (following *Thompson* [1976] and *Friedrich* [1983]). If there is sufficient available energy, then the surface density is increased by entraining the underlying density layer, and the available energy is reduced by the amount used. These energy comparisons are repeated, and the entrainment continued, throughout the water column until there is no remaining available energy to drive further entrainment.

The mixed layer calculations are repeated at subsequent time steps with new imposed values of the solar heating, surface heat, water, and momentum fluxes. If the mixed layer becomes shallower, the density values adjacent to the previous mixed layer are adjusted such that both heat and potential energy are conserved [*Adamec et al.*, 1981].

3.3. Mixed-Layer Cycle

The mixed-layer integration is started at the end of winter and run with hourly time steps at 40.5°N, 26.5°W in the northeast Atlantic (Figure 1; triangle): at this site, the annual heat and water fluxes into the ocean are close to zero [*Woods and Barkmann*, 1986]. The initial ocean profile is taken from the *Robinson et al.* [1979] atlas and the *Topogulf Group* [1986] data. The mixed layer varies seasonally according to the surface forcing (Figure 7): (1) the mixed layer shallows and the temperature increases when there is net surface heating after the spring equinox, (2) the mixed layer reaches its minimum value when the solar heating is a maximum at the summer solstice, (3) the mixed layer subsequently deepens and the temperature continues to increase through late summer until eventually the surface heating becomes less than the cooling from entrainment, and then (4) the mixed layer continues to deepen and cool until the end of winter.

At this chosen site there is good agreement between the model and the climatological observations from the *Robinson et al.* [1979] atlas (crosses in Figure 7). The maximum mixed-layer temperature and depth in the model and observations differ only by 1.2°C and 5 m. These differences may be accounted for by a 10% error in the assumed solar heating, surface cooling, or wind speed. The agreement may be artificially improved by tuning the wind mixing efficiency or the ocean color, but the results are not significantly altered by changing either the penetrative convection factor or the dissipation depth scale.

4. AIR-SEA INTERACTION FOR AN OCEAN EDDY

4.1. Surface Heat and Water Fluxes for an Ocean Eddy

An ocean eddy is modified directly by air-sea interaction and indirectly by an excited secondary circulation (see section 4.2). The modification is investigated by integrating the mixed-layer model for an eddy using the appropriate surface heat and water fluxes. These fluxes depend on (1) the air-sea interaction for the local environment, and (2) the feedback from the eddy surface temperature signal (first and second terms on the right-hand side of equation (10)):

$$\begin{aligned} F_w(2) &= F_w(1) + \rho_a c_e u_a [r_s(2) - r_s(1)] \\ Q_{lc}(2) &= Q_{lc}(1) + \rho_a c_e L_v u_a [r_s(2) - r_s(1)] \\ Q_{sens}(2) &= Q_{sens}(1) + \rho_a c_h C_p u_a [T_s(2) - T_s(1)] \\ Q_{ir}(2) &= Q_{ir}(1) + 4\sigma [T_s(2) - T_s(1)][T_s(1) + 273]^3 \end{aligned} \tag{10}$$

Here, r_s is the specific humidity and T_s is the temperature (in degrees Celsius) at the sea surface, with values for the local environment and eddy indicated by the arguments (1) and (2); the constants are the transfer coefficients c_e and c_h [*Large and Pond*, 1982], the heat capacity of air C_p, the latent heat of evaporation L_v and the Stefan-Boltzmann constant σ. This modification of the eddy does not include the feedback from local changes in the atmospheric boundary layer, as air parcels should remain over the eddy only for a few hours with surface winds of typically 8 m/s.

The evaporative water and latent heat fluxes (equation (10)) may be rewritten in terms of sea surface temperature; the specific humidity is related to the saturated water vapor pressure e_s (in millibars), which is empirically related to sea surface temperature [*Gill*, 1982]:

$$r_s = \epsilon \frac{e_s}{P_a} \left[1 - \frac{e_s}{P_a}(1 - \epsilon) \right]^{-1} \tag{11}$$

$$e_s = 0.98 \times 10^{(a + bT_s)/(1 + cT_s)} \tag{12}$$

Here, P_a is the atmospheric pressure (in millibars) and the coefficients are $a = 0.7859$, $b = 0.03477$, $c = 0.00412$, and $\epsilon = 0.62197$.

The additional surface heat and water fluxes for an eddy with a surface temperature signal of ±2°C are shown in Table 1 for an environment surface temperature of 14.5°C and a mean wind of 8 m/s (using equations (10) to (12)). A cold eddy receives an additional warming of 58 W/m^2 and a freshwater input due to the decrease in evaporation of 1.2 mm/day. In contrast, a warm eddy receives an extra cooling of 80 W/m^2 and a water loss due to the increase in evaporation of 1.5 mm/day. The different flux magnitudes for warm and cold eddies are due to the nonlinear dependence of saturated water vapor on temperature (equation (12)), and the smaller sensible heat transfer coefficient for relatively stable atmospheric conditions.

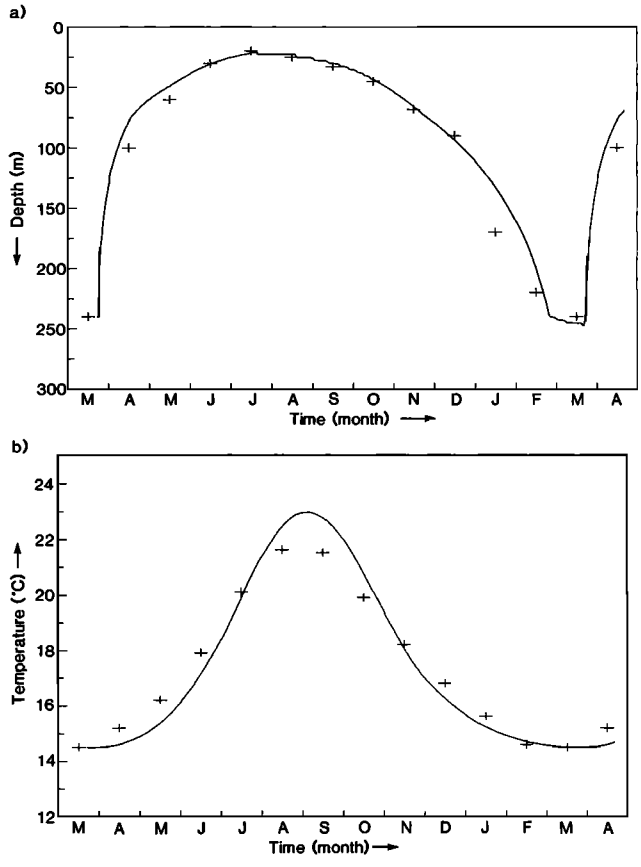

Fig. 7. Annual cycle of (a) mixed-layer depth and (b) temperature at 40.5°N, 26.5°W in the northeast Atlantic: daily model values at 0600 LT (solid line) and *Robinson et al.* [1979] monthly observations (crosses).

4.2. Secondary Velocity Circulation

Air-sea interaction excites a secondary circulation in an eddy. A warm eddy receives additional surface cooling, which produces vertical downwelling and the surface convergence of the cooler surrounding water (Figure 8*a*). A cold eddy, on the other hand, receives extra surface heating, which results in vertical upwelling of cold water (Figure 8*b*). The heat balance of the eddy temperature anomaly (neglecting vertical and lateral mixing here) is given by

$$\frac{\partial T'}{\partial t} = \frac{1}{\rho_o C_w} \frac{\partial Q_a}{\partial z} - u \frac{\partial T'}{\partial r} - w \frac{\partial \overline{T}}{\partial z} \tag{13}$$

An additional surface heating Q_a of 50 W/m^2 over horizontal and depth scales of 30 km and 100 m typically excites a radial flow of $u \sim 0.01$ cm/s and a vertical upwelling of $w \sim 0.02$ m/day (from analytical solutions to the quasi-geostrophic potential vorticity equation [*Williams*, 1987]). Here, r is the radius and ρ_o is the reference density. Assuming horizontal and vertical temperature gradients of 2°C/30 km and 5°C/100 m, then the typical magnitudes of the terms in (13) are

TABLE 1. Additional Surface Heat and Water Fluxes from the Ocean to the Atmosphere for an Eddy with a Surface Temperature Signal of ±2°C

Surface Fluxes	Cold Eddy	Warm Eddy
Q_{le}, W/m^2	−34	44
Q_{sens}, W/m^2	−13	25
Q_{ir}, W/m^2	−11	11
F_w, kg/(s m^2)	-1.4×10^{-5}	1.8×10^{-5}

$$\frac{1}{\rho_o C_w}\frac{\partial Q_a}{\partial z} \sim O(10\times10^{-3}\ ^\circ C/day)$$
$$-u\frac{\partial T'}{\partial r} \sim O(-0.5\times10^{-3}\ ^\circ C/day)$$
$$-w\frac{\partial \bar{T}}{\partial z} \sim O(-1\times10^{-3}\ ^\circ C/day)$$

The temperature change produced by the surface heating is an order of magnitude larger than that from the induced velocity field. The influence of the excited secondary velocity field on the eddy heat balance is therefore neglected here.

4.3. Initial Ocean Eddy Structure

The ocean eddy is assumed to be cylindrically symmetric, with a magnitude and scale which roughly correspond to those of the observed cold-core eddy in section 2 (Table 2). At the start of the mixed-layer integration, the eddy temperature anomaly is chosen to be constant in the winter mixed-layer, and then to exponentially decrease with increasing depth:

$$\begin{aligned} T'(r,z,t=0) &= T_o J_o(kr) & z < -h_o \\ T'(r,z,t=0) &= T_o e^{\nu(z+h_o)} J_o(kr) & z \geq -h_o \end{aligned} \quad (14)$$

The temperature anomaly is assumed to be partially compensated by an opposing salinity anomaly. The initial tangential velocity is given from the thermal-wind balance by

$$\begin{aligned} v(r,z,t=0) &= v_o[1+\nu(z+h_o)]J_1(kr) & z < -h_o \\ v(r,z,t=0) &= v_o e^{\nu(z+h_o)} J_1(kr) & z \geq -h_o \end{aligned} \quad (15)$$

Here, $v_o = -\alpha a_c g k T_o/(\nu f_o)$ is the velocity scale, f_o is the reference Coriolis value, the compensation factor $a_c = 0.5$ for 50% partial compensation, k^{-1} is the eddy horizontal scale of 30 km, ν^{-1} is the temperature anomaly depth scale, and $J_o(kr)$ and $J_1(kr)$ are Bessel functions.

4.4. Mixed-Layer Cycle of an Ocean Eddy

The mixed-layer model for the eddy is started at the end of winter and integrated for 2 years. A warm eddy receives additional cooling due to its surface temperature signal, which gives increased convection and produces a deeper mixed layer (Figure 9). On the other hand, a cold eddy receives extra warming, which produces a shallower mixed layer (Figure 10). These contrasting mixed-layer depths in eddies are observed by the *Ring Group* [1981], *Nilsson and Cresswell* [1981], and *Joyce and Stalcup* [1985].

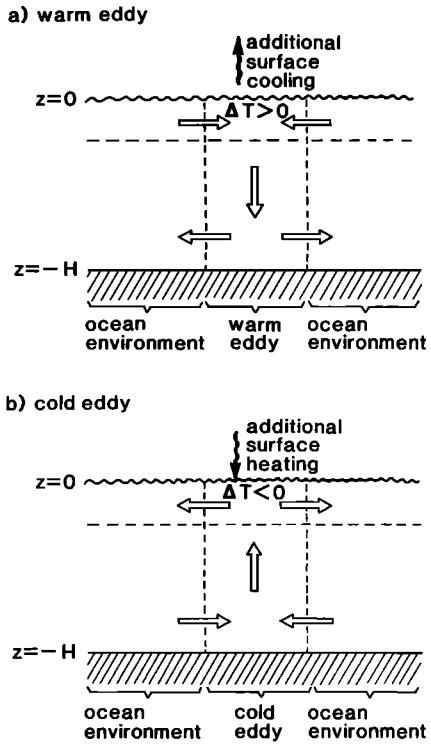

Fig. 8. Schematic cross-section of an eddy showing the secondary velocity circulation excited by air-sea interaction: (a) warm eddy and (b) cold eddy.

Air-sea interaction decreases the initial eddy temperature anomaly and eventually removes the signal in the mixed layer during summer (Figure 11). This shallow mixed layer effectively hides the deeper temperature anomaly from the atmosphere. During this time, satellite infrared observations are unlikely to reveal the eddies. After the summer solstice, however, the mixed layer deepens, and the temperature signal reappears as the deeper anomaly is entrained. The seasonal cycle continues with the buoyancy forcing gradually eroding the temperature anomaly over several years. This seasonal change in the surface temperature signal of an eddy is observed by the *Ring Group* [1981] and is also predicted by the mixed-layer modelling results of *Dewar* [1986].

The temperature signals of the warm and cold eddies are slightly different here due to their contrasting mixed-layer cycles. In the first year, the temperature signal is larger in the warm eddy than in the cold one (Figure 11), since the deeper mixed layer contains a larger proportion of the total temperature anomaly: subsequently, the signal may actually

TABLE 2. Chosen Scales of the Ocean Eddy

Parameter	Variable	Value
Horizontal scale	k^{-1}	30 km
Depth scale	ν^{-1}	500 m
Initial mixed-layer depth	h_o	240 m
Initial temperature anomaly	T_o	±2°C
Initial compensation factor	a_c	0.5
Initial velocity at $z=-h_o$	v_o	∓36 cm/s

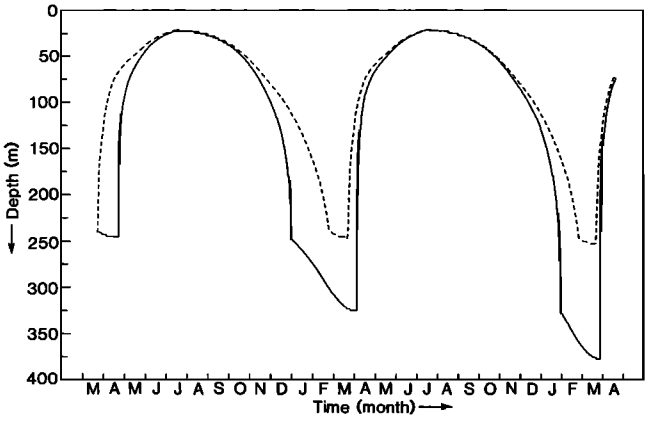

Fig. 9. Mixed-layer depth cycles for 2 years, for a warm eddy (solid line) and the local environment (dashed line).

become smaller in the warm eddy through the increased entrainment of cooler, deeper water.

The salinity of the warm and cold eddies is not significantly altered by the change in the surface water flux due to the presence of the temperature anomaly; this surface flux change only reaches a maximum value of the order of 1 mm/day (section 4.1). The salinity signal is therefore a useful water mass tracer to help identify the origin of features.

The modification of eddies by air-sea interaction is more marked when there are deep mixed layers, due to the larger exposure of the anomaly, than for shallow ones. Eddies should therefore be modified more in winter or at higher latitudes, than in summer or at low latitudes. This is supported by observations of a warm-core ring showing that the rate of its dissipation increased by an order of magnitude during winter [*Okada and Sugimori*, 1986].

5. DYNAMICAL ADJUSTMENT OF AN OCEAN EDDY

5.1. Introduction

Ocean eddies are dynamically modified by buoyancy forcing through the additional surface heat and water fluxes altering the density field. The dynamical changes in the eddy are assessed by coupling the mixed-layer model to a quasi-geostrophic model, and solving the quasi-geostrophic potential vorticity equation:

$$\frac{Dq}{Dt} = \frac{f_o}{\rho_o}\frac{\partial}{\partial z}\left(\frac{B}{N^2}\right) \tag{16}$$

The quasi-geostrophic potential vorticity q consists of (1) relative vorticity ζ, (2) planetary vorticity f, and (3) vortex stretching:

$$q = \zeta + f + \frac{f_o}{\rho_o}\frac{\partial}{\partial z}\left(\frac{1}{N^2}\frac{\partial P'}{\partial z}\right)$$

The buoyancy forcing B drives the dynamical changes in the eddy and is deduced from the mixed-layer integrations. The forcing depends on the modification of the eddy density anomaly by the additional surface heat and water fluxes (equation (10)):

$$B(r,z,t) = -g\frac{\partial}{\partial t}[\rho_2(z,t) - \rho_1(z,t)]\,J_o(kr) \tag{17}$$

Here, D/Dt is the time rate of change following the motion, N is the Brunt-Väisälä frequency, P' is the perturbation pressure, ρ_2 and ρ_1 are the densities of the eddy and the background environment.

The controlling quasi-geostrophic potential vorticity equation (16) is simplified here by assuming the eddy to be cylindrically symmetric, neglecting the nonlinear advection terms and the planetary vorticity gradient to give

$$\frac{\partial}{\partial t}\left(\frac{\partial^2 P'}{\partial z^2} - \gamma\frac{\partial P'}{\partial z} - \left(\frac{Nk}{f_o}\right)^2 P'\right) = \frac{\partial B}{\partial z} - \gamma B \tag{18}$$

where

$$P'(r,z,t) = P'(z,t)J_o(kr) \quad \text{and} \quad \gamma = \frac{2}{N}\frac{dN}{dz}$$

The eddy perturbation pressure field is obtained by solving (18) with rigid-lid upper and lower boundary conditions using the thermodynamic equation:

$$\rho_o N^2 w = B - \frac{\partial}{\partial t}\left(\frac{\partial P'}{\partial z}\right) \tag{19}$$

The imposed Brunt-Väisälä profile is taken from an annual mean profile; the modelled values are chosen to become small but remain nonzero in the mixed layer (whereas in reality they should be zero).

5.2. Tangential Velocity Cycle of an Ocean Eddy

Air-sea interaction alters the tangential velocity of an eddy by driving a secondary velocity circulation (Figure 8). The warm eddy is associated with an initial anticyclonic flow (solid line in Figure 12). Surface cooling induces vertical downwelling, which leads to a surface cyclonic velocity change and a deeper anticyclonic change. Consequently, the anticyclonic flow of the warm eddy is reduced in the surface layer and increased in the deep interior (dashed line in Figure 12).

In contrast, surface heating of the cold eddy induces vertical upwelling and a surface anticyclonic change with a deeper cyclonic motion. Thus the initial cyclonic flow of the cold eddy (solid line in Figure 13) is decreased in the surface layer and increased in the deep interior (dashed line in Figure 13).

Subsurface velocity maxima have often been observed in ocean eddies and rings [*Swallow*, 1971; *Olson*, 1980; *Groupe Tourbillon*, 1983; *Joyce*, 1984]: a subsurface velocity maximum is indeed detected in the cold-core eddy examined in section 2. Over several seasons, air-sea interaction may form

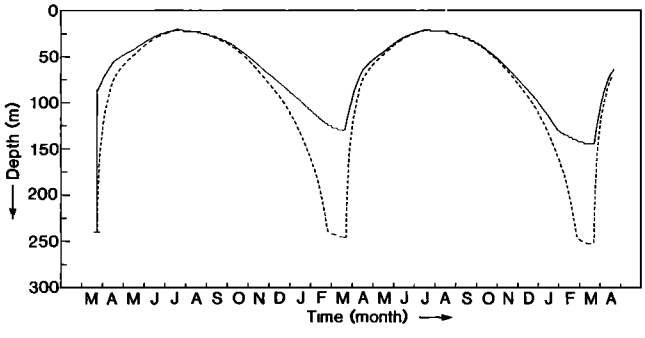

Fig. 10. Mixed-layer depth cycles for 2 years, for a cold eddy (solid line) and the local environment (dashed line).

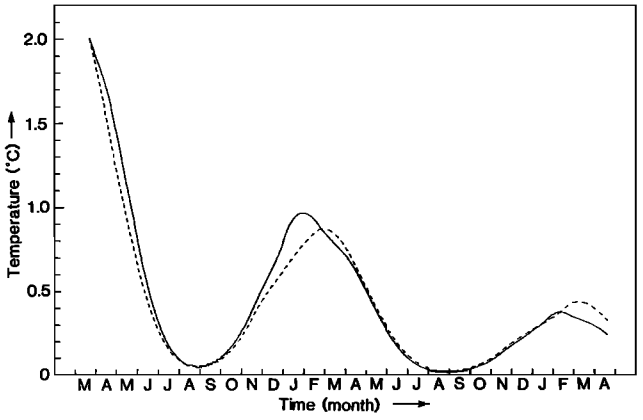

Fig. 11. Surface temperature signal for 2 years, for a warm eddy (solid line) and a cold eddy (dashed line).

these subsurface velocity maxima in warm and cold eddies.

The diabatic forcing does not alter the depth-integrated transport at the level of the quasi-geostrophic approximation; however, the transport may be changed when a cyclostrophic balance is used and the nonlinear advection terms are included. *Dewar* [1987] applies conservation of angular momentun and shows that cooling may in fact increase the transport of an anticyclonic ring through the excited secondary circulation changing the shape and size of the ring.

5.3. Potential Vorticity Cycle of an Ocean Eddy

Air-sea interaction alters the potential vorticity (equation (1)) of the warm and cold eddies by modifying their stratification and relative vorticity in the seasonal boundary layer; this is discussed further for large-scale flow by *Woods* [1985]. The warm eddy initially has smaller potential vorticity values from both its low stratification (increased spacing between σ_t surfaces) and anticyclonic relative vorticity, whereas the cold eddy has larger values (Table 3). Over several seasons, air-sea interaction reduces the eddy temperature and density anomalies. After the following spring shallowing in mixed layer, the eddy stratification becomes

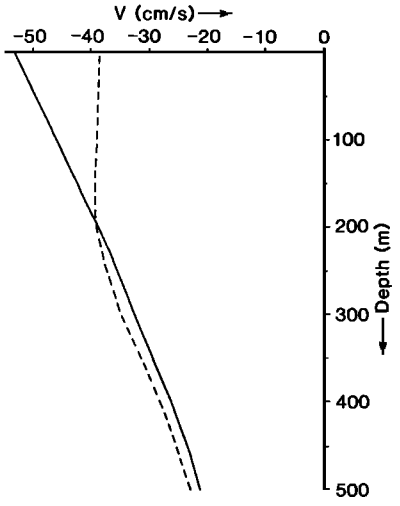

Fig. 12. Tangential velocity profile for a warm eddy: initial profile (solid line) and the profile after 1 year (dashed line).

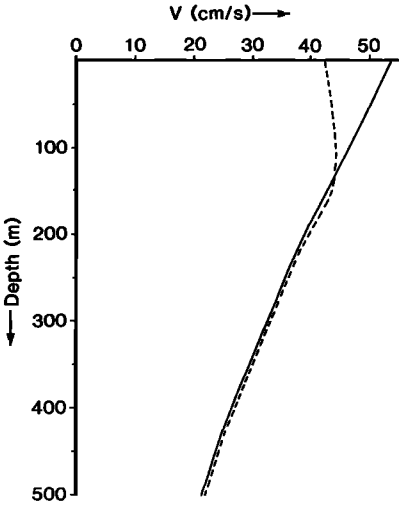

Fig. 13. Tangential velocity profile for a cold eddy: initial profile (solid line) and the profile after 1 year (dashed line).

more similar to that of the environment (Figure 14). In addition, the relative vorticity of the eddy is decreased in magnitude in the surface layer. Air-sea interaction therefore decreases the eddy potential vorticity anomaly in the seasonal boundary layer (Table 3).

The potential vorticity anomaly effectively helps to protect the eddy water mass by inhibiting lateral mixing when diabatic processes are relatively small. The reduction in the potential vorticity anomaly by air-sea interaction may lead to lateral mixing becoming important in eroding any remaining water mass anomaly (such as salinity or chemical tracers) throughout the latter part of an eddy's lifetime.

6. Discussion and Conclusions

Air-sea interaction alters the structure and the life cycle of ocean eddies in the seasonal boundary layer. Eddies are usually formed by internal instability of boundary currents, and they acquire a water mass structure typical of their formation region. When an eddy moves into a different environment, it appears as an anomalous water mass. The eddy is then modified by the local air-sea interaction and the negative feedback from its surface temperature signal. A warm eddy receives additional surface cooling, and a cold eddy experiences additional warming: this produces a deeper mixed layer in a warm eddy and a shallower one in a cold eddy.

TABLE 3. Potential Vorticity along the σ_t =26.3, 26.5 and 26.7 surfaces in July for 2 years (10^{-9} $m^{-1}s^{-1}$)

σ_t	Environment	Warm Eddy	Cold Eddy
		Year 1	
26.3	2.6	1.3	4.7
26.5	1.7	0.4	4.1
26.7	0.6	0.08	3.1
		Year 2	
26.3	2.7	2.2	3.0
26.5	1.7	1.2	2.1
26.7	0.6	0.4	0.4

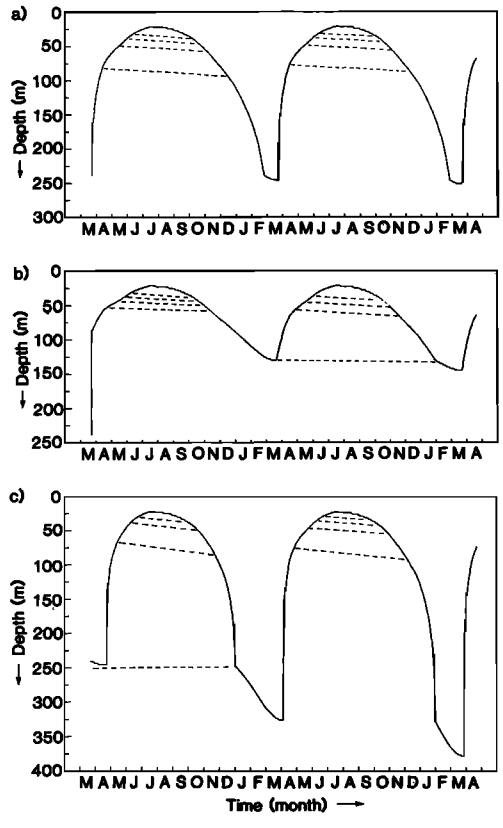

Fig. 14. Mixed-layer cycle and depth of selected σ_t surfaces 26.2, 26.4, 26.6, and 26.8 for 2 years, for (a) local environment, (b) cold eddy, and (c) warm eddy.

Air-sea interaction tends to reduce the eddy temperature anomaly. The surface temperature signal is effectively removed during the summer in the shallow mixed layer. After the summer solstice, however, the mixed layer deepens, and the temperature signal reappears as the underlying anomaly field is entrained. Consequently, satellite infrared observations are more likely to identify and track ocean eddies during winter. Air-sea interaction does not significantly alter the salinity of an eddy, but does reduce its temperature and potential vorticity anomalies. Consequently, salinity is a useful tracer in identifying the origin of features. However, the reduction of the potential vorticity anomaly may eventually allow lateral mixing to become important in eroding the remaining salinity anomaly.

Air-sea interaction alters the eddy velocity profile by driving a secondary velocity circulation. The eddy surface velocity is decreased and the deeper flow is increased; at the level of the quasi-geostrophic approximation there is no change in the depth-integrated circulation. Over several seasons the air-sea interaction may lead to eddies acquiring subsurface velocity maxima; these are often seen in ocean eddy and ring observations.

These modelling predictions are supported by observations of a cold-core eddy in the northeast Atlantic. The observations of the eddy reveal a shallower mixed layer, and a decrease in its temperature signal and velocity field towards the surface. These features may have been formed through air-sea interaction.

The modification of eddies by air-sea interaction is more important in deep mixed layers, typical of winter or high latitudes, than for shallow ones. Air-sea interaction may therefore produce different eddy structures, and perhaps lifetimes, according to the time of year and the eddy path through the ocean.

Acknowledgments. I would like to thank J. D. Woods and the Regionale Ozeanographie Group, Institut für Meereskunde, Kiel, West Germany, for assistance and access to FS *Poseidon* 101b cruise data. I am also grateful to J. G. Harvey and J. C. Marshall for helpful advice and comments. This study was conducted at the University of East Anglia and Imperial College, and was supported by grants from the Natural Environment Research Council and the Admiralty Research Establishment of the United Kingdom.

REFERENCES

Adamec, D., R. L. Elsberry, R. L. Garwood, and R. L. Haney, An embedded mixed-layer ocean circulation model, *Dyn. Atmos. Oceans, 2*, 69–96, 1981.

Baumgartner, A., and E. Reichel, *The World Water Balance*, 179 pp., Elsevier, Amsterdam, 1975.

Budyko, M. I., *Climate and Life*, 508 pp., Academic, San Diego, Calif., 1974.

Bunker, A. F., Computations of surface energy flux and annual air-sea interaction cycles of the North Atlantic, *Mon. Weather Rev., 104*, 1122–1140, 1976.

Colin de Verdiere, A., J. G. Harvey, and M. Arhan, Stirring and mixing of thermohaline anomalies, *J. Mar. Res., 44*, 93–118, 1986.

Davey, M. K., and P. D. Killworth, Isolated waves and eddies in a shallow water model, *J. Phys. Oceanogr., 14*, 1047–1064, 1984.

Dewar, W. K., Mixed layers in Gulf Stream rings, *Dyn. Atmos. Oceans, 10*, 1–29, 1986.

Dewar, W. K., Ventilating warm rings: Theory and energetics, *J. Phys. Oceanogr., 17*, 2219–2231, 1987.

Dickson, R. R., On the relationship between ocean transparency and the depth of sonic scattering layers in the North Atlantic, *J. Cons. Int. Explor. Mer., 34*(3), 416–422, 1972.

Dorman, C. E., and R. H. Bourke, Precipitation over the Atlantic Ocean, 30°S to 70°N, *Mon. Weather Rev., 109*, 554–563, 1981.

Friedrich, H., Simulation of the thermal stratification at the FLEX central station with a one-dimensional integral model, in *North Sea Dynamics*, edited by J. Sündermann, 693 pp., Springer-Verlag, New York, 1983.

Gill, A. E., *Atmosphere-Ocean Dynamics*, 662 pp., Academic, San Diego, Calif., 1982.

Gill, A. E., and J. S. Turner, A comparison of seasonal thermocline models with observation, *Deep Sea Res., 23*, 391–401, 1976.

Gill, A. E., J. S. A. Green, and A. J. Simmons, Energy partition in the large-scale ocean circulation and the production of mid-ocean eddies, *Deep Sea Res., 21*, 499–528, 1974.

Groupe Tourbillon, The Tourbillon Experiment: A study of a mesoscale eddy in the eastern North Atlantic, *Deep Sea Res., 30*, 475–511, 1983.

Horch, A., W. Barkmann, and J. D. Woods, Die Erwärmung des Ozeans hervorgerufen durch solare Strahlungsenergie, *Ber. Inst. Meereskd. Univ. Kiel, 120*, 190 pp., 1983.

Joyce, T. M., Velocity and hydrographic structure of a Gulf Stream warm core ring, *J. Phys. Oceanogr., 14*, 936–947, 1984.

Joyce, T. M., and M. C. Stalcup, Wintertime convection in a Gulf Stream warm core ring, *J. Phys. Oceanogr., 15*, 1032–1042, 1985.

Kato, H., and O. M. Phillips, On the penetration of a turbulent layer into a stratified layer, *J. Fluid Mech., 37*, 643–655, 1969.

Kraus, E. B., and J. S. Turner, A one-dimensional model of the seasonal thermocline, II, The general theory and its consequences, *Tellus, 19*, 19–105, 1967.

Large, W. G., and S. Pond, Open ocean momentum flux measurements in moderate to strong winds, *J. Phys. Oceanogr., 11*, 324–336, 1981.

Large, W. G., and S. Pond, Sensible and latent heat flux measurements over the ocean, *J. Phys. Oceanogr., 12*, 464–482, 1982.

Leach, H., P. J. Minnett, and J. D. Woods, The GATE Lagrangian Batfish experiment, *Deep Sea Res., 32*, 575–597, 1985.

Leach, H., N. Didden, V. Fiekas, J. Fischer, A. Horch, and J. D. Woods, Sea Rover data report II North Atlantic summer 1983, *Ber. Inst. Meereskd. Univ. Kiel, 175*, 91 pp., 1987.

List, R. J., *Smithsonian Meteorological Tables*, Smithsonian Institution., Washington, D. C., 1966.

McDowell, S., P. B. Rhines, and T. Keffer, North Atlantic potential vorticity and its relation to the general circulation, *J. Phys. Oceanogr., 12*, 1417–1436, 1982.

Müller, P., and C. Frankignoul, Direct atmospheric forcing of geostrophic eddies, *J. Phys. Oceanogr., 11*, 287–308, 1981.

Niiler, P. P., and E. B. Kraus, One-dimensional models of the upper ocean, in *Modelling and Prediction of the Upper Layers of the Ocean*, edited by E. B. Kraus, 325 pp., Pergamon, Elmsford, N. J., 1977.

Nilsson, C. S., and G. R. Cresswell, The formation and evolution of East Australian current warm-core ring eddies, *Prog. Oceanogr., 9*, 133–183, 1981.

Okada, Y., and Y. Sugimori, Decay of warm-core rings based on observations of available potential energy, *Deep Sea Res., 33*, 1577–1599, 1986.

Olson, D. B., The physical oceanography of two rings observed by the cyclonic ring experiment, II, Dynamics, *J. Phys. Oceanogr., 10*, 514–528, 1980.

Payne, R. E., Albedo of the sea surface, *J. Atmos. Sci., 29*, 959–970, 1972.

Richardson, P. L., Gulf Stream rings, in *Eddies in Marine Science*, edited by A. R. Robinson, 609 pp., Springer-Verlag, New York, 1983.

Ring Group, Gulf Stream cold-core rings: Their physics, chemistry and biology, *Science, 212*, 1091–1100, 1981.

Robinson, M. K., R. A. Bauer, and E. H. Schroeder, *Atlas of North Atlantic-Indian Ocean Monthly Mean Temperatures and Mean Salinities of the Surface Layer*, U.S. Naval Oceanographic Office, Washington, D. C., 1979.

Schmitt, R. W., and D. B. Olson, Wintertime convection in warm-core rings: Thermocline ventilation and the formation of mesoscale lenses, *J. Geophys. Res., 90*, 8823–8837, 1985.

Swallow, J. C., The Aries current measurements in the western North Atlantic, *Philos. Trans. R. Soc. London, Ser. A, 270*, 451–461, 1971.

Thompson, R. O. R. Y., Climatological numerical models of the surface mixed layers of the ocean, *J. Phys. Oceanogr., 6*, 496–503, 1976.

Topogulf Group, A joint programme initiated by IFREMER, Brest (France), IFM, Kiel (W. Germany) Data Report, Volume 1: CTD, O_2 and Nutrients, *Ber. Inst. Meereskd. Univ. Kiel, 154*, 183 pp., 1986.

Wells, N. C., A coupled ocean-atmosphere experiment: the ocean response, *Q.J.R. Meteorol. Soc., 105*, 355–370, 1979.

Williams, R. G., The influence of air-sea interaction on ocean synoptic-scale eddies, Ph.D. thesis, Univ. of East Anglia, Norwich, England, 1987.

Woods, J. D., The warm water sphere of the northeast Atlantic: A miscellany, *Ber. Inst. Meereskd. Univ. Kiel, 128*, 39 pp., 1984.

Woods, J. D., Physics of thermocline ventilation, in *Coupled Atmosphere-Ocean Models*, edited by J. C. J. Nihoul, Elsevier, Amsterdam, 1985.

Woods, J. D., and W. Barkmann, The response of the upper ocean to solar heating, I, The mixed-layer, *Q.J.R. Meteorol. Soc., 112*, 1–27, 1986.

R. G. Williams, Space and Atmospheric Physics Group, Department of Physics, Imperial College of Science and Technology, Blackett Laboratory, Prince Consort Road, London, SW7 2BZ England.

(Received January 25, 1988;
accepted April 7, 1988.)